symmetry

MDPI

Review

Nuclear Symmetry Energy in Strongly Interacting Matter: Past, Present and Future

Jirina R. Stone [1,2]

[1] Department of Physics (Astrophysics), University of Oxford, Oxford OX1 3RH, UK; jirina.stone@physics.ox.ac.uk
[2] Department of Physics and Astronomy, University of Tennessee, Knoxville, TN 37996, USA

Abstract: The concept of symmetry under various transformations of quantities describing basic natural phenomena is one of the fundamental principles in the mathematical formulation of physical laws. Starting with Noether's theorems, we highlight some well–known examples of global symmetries and symmetry breaking on the particle level, such as the separation of strong and electroweak interactions and the Higgs mechanism, which gives mass to leptons and quarks. The relation between symmetry energy and charge symmetry breaking at both the nuclear level (under the interchange of protons and neutrons) and the particle level (under the interchange of u and d quarks) forms the main subject of this work. We trace the concept of symmetry energy from its introduction in the simple semi-empirical mass formula and liquid drop models to the most sophisticated non-relativistic, relativistic, and *ab initio* models. Methods used to extract symmetry energy attributes, utilizing the most significant combined terrestrial and astrophysical data and theoretical predictions, are reviewed. This includes properties of finite nuclei, heavy-ion collisions, neutron stars, gravitational waves, and parity–violating electron scattering experiments such as CREX and PREX, for which selected examples are provided. Finally, future approaches to investigation of the symmetry energy and its properties are discussed.

Keywords: symmetry and conservation laws; symmetry breaking; semi–empirical mass formula; liquid drop model; heavy-ion collisions; neutron skin; neutron stars; quark matter

Citation: Stone, J.R. Nuclear Symmetry Energy in Strongly Interacting Matter: Past, Present and Future. *Symmetry* **2024**, *16*, 1038. https://doi.org/10.3390/sym16081038

Academic Editors: Odilon Lourenço, Helena Sofia Pais and Mariana Dutra

Received: 22 April 2024
Revised: 6 June 2024
Accepted: 8 June 2024
Published: 13 August 2024

1. Introduction

The concept of symmetry with respect to the transformation of quantities describing basic natural phenomena is one of the guiding principles of the mathematical formulation of physical laws. It is difficult to trace where it originated, but one should certainly mention the work of Emmy Noether, who in 1918 proved two theorems stating that continuous symmetries in the universe give rise to mathematical conservation laws [1,2]. These theorems [3,4] became central in general relativity, quantum physics and elementary particle physics. In simple terms, her work implies that, for example:

- Translation invariance (symmetry) leads to the conservation of linear momentum.
- Rotation invariance in space yields the conservation of angular momentum.
- Invariance with respect to time-reversal results in the conservation of energy.
- U(1) local symmetry with respect to the phase shift in rotation by a certain angle in a complex plane gives rise to the conservation of the electric charge; in the Standard model, U(1) symmetry leads to the conservation of the weak charge, a combination of the electric charge and isospin.
- Invariance under a combined replacement of all particles in a system by their antiparticles (Charge), their mirror images (Parity) and reversal of the flow of time (Time) constituting the CPT theorem [5], which is an example of a discrete symmetry. The total symmetry holds in the Standard model [https://www.iop.org/explore-physics/big-ideas-physics/standard-model (accessed on 1 March 2024)] but not for individual

components. The related conservation law is still a matter of debate, but this does not diminish the importance of CPT invariance in theoretical physics [6].

The discovery of various mechanisms of symmetry breaking in the 1960's and 1970's (see [7] for the most recent review) represented a major breakthrough in the investigation of symmetries in nature and the consequences of their breaking. It is now believed that most symmetries, existing at some point in the evolution of the universe, are now broken. This means they ceased to exist due to the interference of some external conditions and can be (partially) restored if these conditions change.

For example, in cosmology, the cooling of the universe led to separation of the strong force from the electroweak interaction at some very high temperature, higher than the critical temperature for the separation of the electromagnetic and weak interactions. Further cooling caused the breaking of the electroweak symmetry, with the electromagnetic and weak forces acquiring very different strengths and properties. If the temperature in some terrestrial experiment increased toward the value at the birth of the universe, partial restoration of the original unified force might be possible.

Another example of the consequences of spontaneous symmetry breaking is the Higgs mechanism [8] based on the assumption that at the beginning of the universe, there existed a scalar field present in all space (the Higgs field) in an unstable state. Spontaneous symmetry breaking of the Higgs field triggered a mechanism that gave mass to elementary fermions (quarks and leptons), the weak bosons W and Z and to the Higgs boson itself.

The symmetry and its breaking directly relevant to this work is the approximate charge symmetry under global exchange of u and d quarks, reflecting conservation of the strong force with respect to this exchange. We will discuss charge symmetry and the consequences of its breaking in low- and high-energy nuclear physics in the next sections.

This paper is organized as follows: The paper is organized as follows: After a general introduction to the concept of symmetry and its breaking in physics in Section 1, the symmetry energy phenomenology is discussed in Section 2, including introduction of isospin (Section 2.1) and symmetry energy in infinite matter and finite nuclei via liquid drop models (Sections 2.2 and 2.3). Section 3 is devoted to a survey of experimental efforts to determine the properties of symmetry energy in dedicated systems including mirror nuclei (Section 3.1), heavy-ion collisions (Section 3.2), measurement of neutron skin (Section 3.3) and combined terrestrial and astrophysical data (Section 3.4). Finally, conclusions and outlook are presented in Section 4.

This review makes no attempt to give a detailed description of the many methods and approaches mentioned. For these, the reader is directed to the references provided and any good basic text.

2. Symmetry Energy Phenomenology

2.1. Charge Symmetry and Conservation of Isospin

The idea that the proton and the neutron are two charge states of one particle, the nucleon, was proposed by Heisenberg in 1932 [9]. This concept, supported by experimental data from p-p and p-n scattering, led to the introduction of a quantity locally conserved in nucleon–nucleon interactions, initially referred to as "isotopic spin" and later called "isospin" by Wigner in 1937 [10]. In 1954, Yang and Mills showed that the conservation of isospin is a global property of strong interactions and is generated by symmetry under independent rotation of isospin at all space–time points, provided the electromagnetic field is neglected (see [11] and refs. therein).

The formulation of quantum chromodynamics (QCD), the theory of strong interactions, relates isospin conservation to charge symmetry. This symmetry is not exact but is broken by the competition of two effects, the non-equal u and d quark masses and their different charges. It turns out that the mass difference between u and d quarks has an effect about twice as strong as that of their electromagnetic repulsion, making it the dominant factor in charge symmetry breaking. The reasons for the different masses of the u and d quarks and why they possess mass at all are not yet fully understood. Quark masses cannot be

measured directly because as far as is known, they cannot exist freely; they are always bound to particles. Both indirect experiments and lattice QCD suggest that quark masses in hadrons are less than about 6 MeV/c^2. It is conjectured that the quarks contribute very little to hadron masses (with nucleon mass being about 940 MeV/c^2), which mostly come from the strong interaction through processes such as emission and absorption of gluons via the energy–mass equivalence.

Assuming that the masses of *u* and *d* quarks are zero, another important symmetry of the strong interaction in hadronic systems can be identified as symmetry under the reversal of the quark spin orientation with respect of the direction of its motion, known as the chiral symmetry [12]. This symmetry is both explicitly and spontaneously broken in nature. Small quark masses and electroweak forces are responsible for the explicit breaking. Spontaneous chiral symmetry breaking contributes to generating the masses of hadrons and making pseudoscalar mesons (e.g., the pion) light. As the theory of strong interaction cannot be directly applied in low-energy nuclear physics, chiral effective field theories are used to model systems composed of nucleons and pions, both finite and infinite, and to probe the long-range part of the nuclear force [12–16].

2.2. Infinite Matter, Finite Nuclei and Symmetry Energy

As already mentioned in Section 2.1, the roles of isospin and of the proton/neutron ratio in practical low-energy nuclear physics were recognized early in the 20th century. The quest for understanding the mechanism of nuclear binding led to the formulation of the semi–empirical mass formula (SMF), which is based on the incompressible liquid drop model of the atomic nucleus, constructed by Gamow in 1930 [17] and later developed by Weizsacker [18] and Bethe and Bacher [19] in 1935 and 1936, respectively.

In this model, the binding energy per particle of a spherical nucleus with $A = N + Z$ nucleons, consisting of closely packed spherical N neutrons and Z protons, is given by

$$B(A,Z)/A = a_{\mathrm{vol}} + a_{\mathrm{surf}}A^{-1/3} + a_{\mathrm{C}}Z^2A^{-4/3} + a_{\mathrm{sym}}(N-Z)^2A^{-2}, \quad (1)$$

where a_{vol} is expected to be positive and the other three coefficients, a_{surf}, and a_{C} and a_{sym} are negative [20]. The first three terms, representing the volume, surface, and Coulomb contributions to $B(A,Z)/A$, respectively, have classical forms. The energy associated with charge symmetry breaking at the nucleon level is included in the symmetry term with the coefficient a_{sym}. This term is constructed with the assumption that protons and neutrons are fermions with different values of isospin, form non-interacting Fermi gases and obey the Pauli principle. The coefficients in Equation (1) are determined by fitting to the measured nuclear masses $M(A,Z) = Zm(^1H) + Nm_{\mathrm{n}} - B(A,Z)/c^2$ [20]. The A dependence of individual terms in Equation (1) is illustrated in Figure 1. As expected, the interplay between the surface and Coulomb terms is dependent on A, while the symmetry term is contributing around 25% to $B(A,Z)/A$ almost independently of A (except for very light nuclei) across the whole range of A between about 50 and 300.

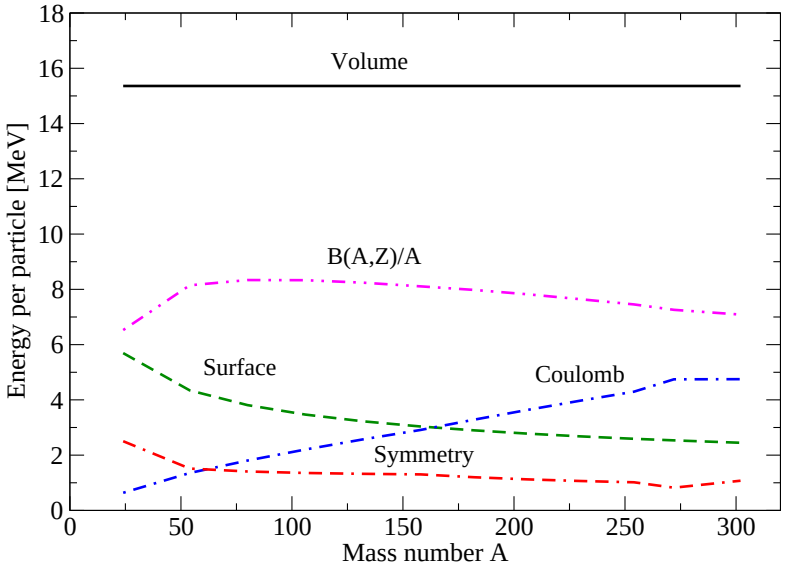

Figure 1. Binding energy per particle as calculated in Equation (1) with coefficients a_{vol}, a_{surf}, a_{C} and a_{sym} equal to 15.36 MeV, −16.42 MeV, −0.691 MeV and −22.53 MeV, respectively. The relative magnitude of the volume, surface, Coulomb and symmetry terms is displayed versus the mass number $A = Z + N$ for a range of $(Z, N) = (8, 16), (20, 34), (30, 50), (40, 66), (50, 82), (60, 98), (70, 112), (80, 126), (90, 140)$ and $(100, 154)$. N = Z nuclei are not included in the figure, illustrating only a general trend. For more discussions, see the text and Ref. [21].

The mass number independence of the volume term in Equation (1) led to the concept of infinite nuclear matter (INM), originally a platform for testing nuclear models under simplified conditions [19,22]. INM consists of an infinite number of uniformly distributed protons and neutrons, with a fixed proton/neutron ratio and no Coulomb field. Only two quantities characterize INM, the binding energy per particle E_0 and the particle number density ρ_0. Extrapolation of $B(A, Z = N)/A$ to $A \to \infty$ approximates E_0, determined by fit to experimental atomic masses, to be close to -16 MeV [20].

More assumptions were needed to calculate the value of the second quantity describing INM, the particle number density ρ_0 [21]. As SMF assumes a spherical nucleus of radius R with closely packed spherical nucleons of radius r_0 uniformly distributed inside, the density of such an object can be calculated using a relation between R, r_0 and the number of nucleons A. The volume of a sphere with radius R containing A smaller spheres with radii r_0 is $V = \frac{4}{3}\pi R^3$, whichf is equal to $\frac{4}{3}\pi r_0^3 f A$. Introducing $R_0 = f r_0$ (f being a packing factor), we obtain the familiar expression for the mass number dependence of the nuclear radius $R = R_0 A^{1/3}$ and the A-independent uniform density $\rho_0 = A/V = 3/(4\pi R_0^3)$.

In the early days, the value of R_0 was determined from the analysis of electron scattering experiments on heavy nuclei and on hydrogen and the deuteron, which confirmed the finite size of the nucleon. This analysis was not quite model-independent because it required assumptions about the proton charge distribution in the nucleus [23,24]. Eventually, R_0 = 1.12 fm was chosen and ρ_0 set to 0.17 fm^{-3} [22].

Including this elementary algebra in the paper is important in the spirit of searching for the origin of quantities that are now in everyday use as benchmark requirements of nuclear theory models but clearly have a fundamental physical content despite all its limits.

There are two extreme forms of INM: symmetric nuclear matter (SNM), consisting of an equal number of protons (uud) and neutrons (ddu); and pure neutron matter (PNM), made only of neutrons. SNM and PNM are extremely well suited for the determination of the symmetry energy and its relation to charge symmetry and its breaking [25].

If charge symmetry were exact, all nucleons would have the same mass and zero charge, and INM would in the PNM phase, i.e., a fully symmetric excited state of nuclear matter. However, as all systems in nature prefer being in the lowest possible state, a

spontaneous charge symmetry breaking occurs, driving the INM to its ground state, which is in equilibrium with respect to exchange $d \leftrightarrow u$, having, on average, an equal number of protons and neutrons at each space-time point, the SNM. This transition is mainly assisted by the difference between d and u quark masses but also with their different charges, as discussed in the previous section. The energy difference between PNM and SNM binding energies per particle at saturation density is a measure of the charge symmetry breaking at nuclear level and is defined as symmetry energy S_0,

$$S_0 = [B(A, Z = 0)/A - B(A, Z = N)/A]_{A\to\infty}, \quad (2)$$

which leads to the approximation of S_0 by $a_{\rm sym}$. Here, the symbol S_0 has a special meaning, representing the symmetry energy per particle at the saturation density. Despite various refinements of the SMF formula, including correlations between individual terms and different methods of fitting to experimental atomic masses, $a_{\rm sym}$ is found with a most likely value ≈ 30 MeV [20].

In this section, we emphasize that the parameters of INM and their implications are based only on measured atomic masses and electron scattering experiments but otherwise on very basic assumptions about properties of a hypothetical nuclear medium stripped of any realistic effects such as surface tension, Coulomb force and pairing. Yet, a fundamental outcome arises: the constant particle number density (independent of the nucleon number A) implies equilibrium between the attractive and repulsive components of the nuclear force at that density, known as the *saturation density* . In other words, regardless of the position in space, each nucleon is surrounded by roughly the same number of neighboring nucleons. If the range of the nuclear force is shorter than the average distance between nucleons, each nucleon interacts with only a few neighboring nucleons and contributes equally to the total binding energy per particle of the matter, the *saturation energy*. We reiterate that the early values of E_0, ρ_0 and S_0 are remarkably close to those presently used in current sophisticated models. We will return to this point in the conclusions in Section 4.

2.3. Density Dependence of the Symmetry Energy and the Liquid Drop Models

As concluded in the previous section, the SMF apparently grasped important phenomenology of nuclear binding at just one density, the saturation density, in the most trivial case of a spherical nucleus with uniform distributions of spherical protons and neutrons; further development was clearly desirable. Myers and Swiatecki [26–28] developed in the 1960's and early 1970's, a series of models still based on the liquid drop/droplet concept but which included more realistic features to calculate nuclear masses. These models retained the basic ingredients, volume, surface, Coulomb and symmetry terms, but each was developed further. First, the SMF was extended to include dependence on nuclear shape and shell corrections to form a Liquid Drop Model (LDM) [26]. Next, the Droplet Model of average nuclear properties was derived by expanding volume, surface and Coulomb terms in a Taylor series around their values in the LDM. This model allowed, together with the aid of an independent Thomas–Fermi model, the calculation of a variety of nuclear properties, such as nuclear radii, proton and neutron density distributions, neutron skin, nuclear compression and the surface and volume symmetry energy [27].

In this section, we follow the 1969 version of the Droplet Model [27], which consistently demonstrates the transition from the SMF to a density-dependent model of nuclear masses and thus nuclear ground-state binding. The essential point is that the Taylor expansions in this model are performed in terms of two variables, the neutron–proton (n-p) asymmetry $\delta = (\rho_{\rm n} - \rho_{\rm p})/\rho$ (with $\rho = \rho_{\rm n} + \rho_{\rm p}$) and the deviation of the density ρ from the saturation density ρ_0 $\varepsilon = -(\rho - \rho_0)/(3\rho_0)$. It follows that the model explicitly includes sensitivity to ranges of values of δ and ε within which it is employed.

Taking only the volume term of the energy density in the Droplet Model, the binding energy per particle of nuclear matter is now expressed as [27]

$$B(\rho, \delta, \varepsilon)/A = -a_{\rm vol} + J\delta^2 + 1/2(K\varepsilon^2 - 2L\varepsilon\delta^2 + M\delta^4) + \ldots \quad (3)$$

in powers of ε and δ^2 (assuming symmetry between neutrons and protons) where J is the symmetry energy coefficient, K is the compressibility coefficient, and the term with L determines the density dependence of the symmetry energy chosen that L is always positive. The symmetry anharmonicity coefficient M specifies deviation of the symmetry energy from a quadratic dependence on δ. We note that the sign of a_{vol} in Equation (3) is opposite to that in Equation (1) in line with the original reference.

At the saturation density, δ and ε are zero in SNM and the binding energy per particle is

$$B(\rho, \delta = 0, \varepsilon = 0)/A = E_0. \tag{4}$$

The energy per particle of PNM at saturation when δ = 1 and ε = 0 becomes

$$B(\rho, \delta = 1, \varepsilon = 0)/A = E_0 + J + 1/2M, \tag{5}$$

where M represents a second-order contribution often neglected in other models. At any other density, Equation (3) allows the introduction of *asymmetric* nuclear-matter (ANM) with a density and proton/neutron ratio dependent energy per particle.

The symmetry energy per particle at saturation density S_0 (see Equation (2)) is now equal to J, with a small higher-order contribution $S_0 = J + 1/2M$. At any other density, the difference between binding energies per particle of PNM and SNM becomes $S = J - L\varepsilon + 1/2M$.

The use of Taylor expansions raises questions about their validity, especially at densities and n-p asymmetries far from saturation values. To examine limits on such a strategy, we rewrite Equation (3) as

$$E = E_1 + E_2 + E_3 \tag{6}$$

with

$$E_1 = -a_{vol}, \tag{7}$$
$$E_2 = J\delta^2, \tag{8}$$
$$E_3 = 1/2(K\varepsilon^2 - 2L\varepsilon\delta^2 + M\delta^4). \tag{9}$$

Examination of Figure 2 reveals that while E_2 is dependent only on δ, which is the usual approximation in practice, E_3, the only part dependent on both ε and δ as well as on K and L, will influence the nuclear binding of asymmetric systems further away from ρ_0. Although at saturation density (middle panel) its contribution is negligible, and the series (3) converges rapidly, at densities below saturation E_3 reduces the effect of E_2, driving the system to stronger binding (top panel). The opposite effect is seen at densities above saturation (bottom panel). Already at twice ρ_0, the positive contribution of E_3 to the total binding energy, higher than that of E_2, indicates divergence of the series (3). It increases significantly the binding energy of neutron-rich nuclei and, consequently, that of PNM. Given the definition of symmetry energy using PNM and SMN, the effect of E_3 is significant and should not be neglected at densities higher than $2\rho_0$.

For completeness, it should be noted that further extension of liquid-drop-based physics to finite nuclei led to the series of macroscopic–microscopic droplet models, such as the finite range droplet model (FRDM) of Moller and collaborators ([29–31] and that of the referebces therein). These models are currently providing some of the most reliable empirical predictions not only of nuclear masses but also nuclear shapes, fission barriers and α and β decay rates.

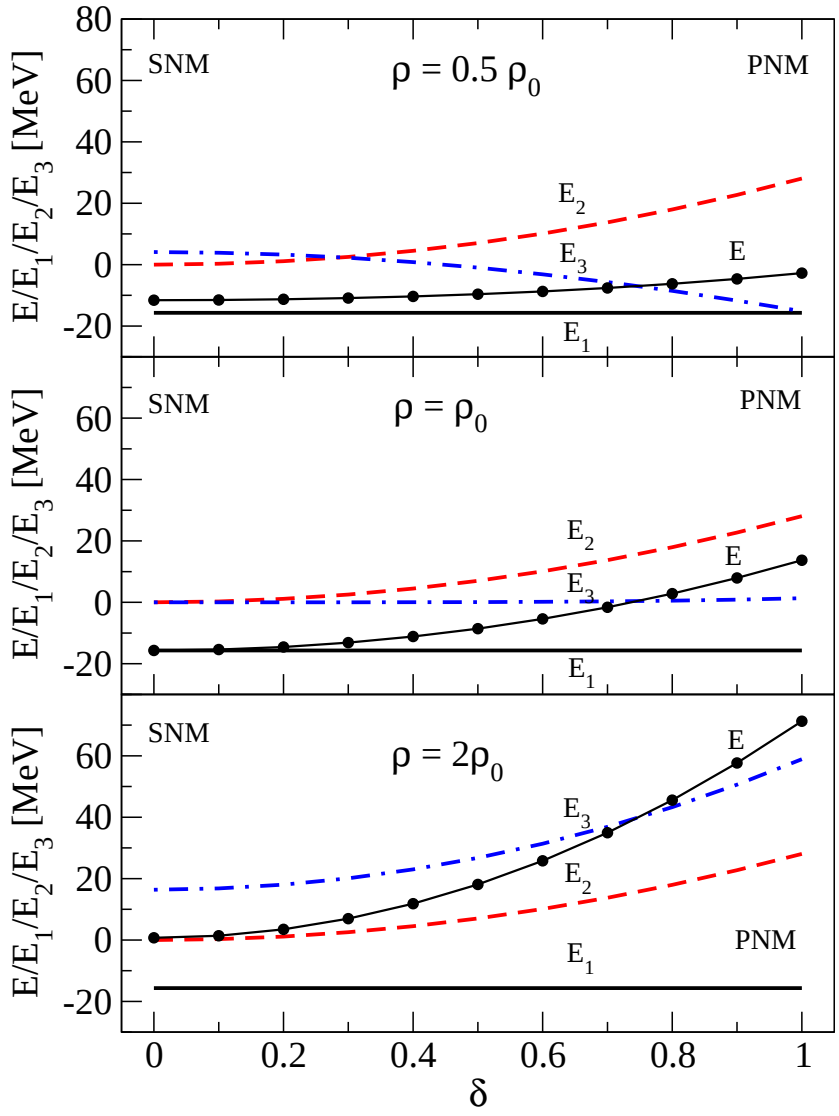

Figure 2. Energy E (full black circles) vs. asymmetry δ spanning from symmetric ($\delta = 0$) to pure neutron matter ($\delta = 1$). The individual terms E_1 (solid black), E_2 (dashed red) and E_3 (dot-dashed blue) were calculated with $a_{\rm vol}$, J, K, L and M being equal 15.677, 28.062, 294.80, 123.53 and 2.673 MeV, respectively [27], for three values of the density 0.5, 1 and $2\rho_0$, corresponding to ε = 0.167, 0 and -0.333 (top, middle and botton panel), respectively.

However, neither SMF nor various liquid-drop-based models include assumptions on nuclear interactions affecting nuclear binding. We discuss this topic, which triggered a wide-spread activity in the field of low-energy nuclear physics, in the next section.

3. Search for the Symmetry Energy

The quest for constraining the symmetry energy and its properties has been one of the main topics of interest in nuclear structure theory and experiments in recent decades. Comprehensive review articles have summarized the state of relevant data and theory at the time they were written [16,32–38]. Despite consolidated efforts, fundamental challenge remains due to the fact that symmetry energy is not a directly measurable quantity but must be extracted from rather convoluted data using nuclear and particle models. It is close to impossible to include adequately all the correlations among the model parameters and take into account different sensitivity and uncertainty in the data. Thus, unique identification of the symmetry energy related to the charge symmetry breaking and its contribution to understanding of nuclear forces is currently beoynd reach. What is equally challenging is to

give justice to the extensive activity in this field. Thus, we give only a few recent examples to illustrate the breadth and diversity of the search for symmetry energy, its properties and influence in various physical systems.

3.1. Charge Symmetry Breaking and Mirror Nuclei

In Section 2.2, we discussed the basic definition of the symmetry energy, S_0, as a difference between SNM and PNM energies per particle at saturation density as an example of the charge symmetry breaking in INM. Charge symmetry and charge independence of nuclear forces in finite nuclei have been extensively studied in mirror nuclei, i.e., pairs of nuclei with with exchanged proton and neutron numbers, for example, ^{15}O and ^{15}N, ^{17}O and ^{17}F, ^{39}Ca and ^{39}K or ^{41}Sc and ^{41}Ca. The discrepancy between experiment and theory in the binding and Coulomb energy differences of mirror pairs was identified in the 1960's and is known as the Okamoto–Nolen–Schiffer anomaly (ONS) [39,40]. It remains one of the long-standing problems in nuclear physics.

To parameterize charge symmetry breaking in finite nuclei and its consequence for ONS, various theoretical models have been utilized in the past, e.g., [41–46] and most recently by Li et al. [47]. The models include charge symmetry breaking short-range interactions and long-range electromagnetic interaction on various level of sophistication. Models including effects of quark structure of nucleons were also explored, in e.g., [25,48] and very recently by Sagawa et al. [49] who proposed a phenomenological model providing a link between charge symmetry breaking of the nuclear interaction and QCD.

However, although some of the models yielded results rather close to experiment, a full understanding of the ONS anomaly leading to improved modeling of charge symmetry breaking in nuclei is still elusive.

3.2. Heavy-Ion Collisions

Heavy-ion collisions (HIC) at low and medium beam energy (below about 10 GeV/nucleon) have been considered for a long time the only terrestrial means to explore the density dependence of the symmetry energy in the supra-saturation density region and to utilize it to improve our knowledge of the nuclear equation of state (EoS). In this section, we focus on the current status of the effort to extract properties of nuclear matter at various densities, temperatures and isospin asymmetries and to relate the predictions from nuclear many-body theory to observables measured in medium-energy collisions.

Data from elliptic and transverse particle flows, isospin diffusion in peripheral collision, near–threshold pion production and n-p spectra and/or measurements of the π^-/π^+ ratio (see e.g., [50–59]) have been utilized and analyzed using two classes of transport codes, one based on Boltzmann–Uehling–Uhlenbeck (BUU) theory [60,61] and the other on quantum molecular dynamics [62] (comparisons of the outcome of both methods can be found in [63–65]).

The data are usually analysed using a set of models with systematically different density dependence (slopes) of symmetry energy, quantified by the derivative of the symmetry energy with respect to density at saturation, the parameter L, important for construction of the EoS of high-density matter. In simpler cases, just two models are used, one predicting up-sloping (stiff) and the one down-sloping (soft) rate of change of the symmetry energy with increasing density [63] and agreement with experiment is sought.

The questions which are still debated in the community are what is the maximum total density achievable in a n-p matter in low and medium HIC and whether the EoS, reflecting HIC data obtained in this region, is applicable in neutron stars (NS).

Maximal total particle density in n-p matter created in collisions of symmetric and asymmetric Ca, Sn and Pb systems at beam energies below 800 MeV/nucleon was investigated by Stone et al. [66–68]. The pBUU transport model [50] was used with two Skyrme forces, SVbas (soft) and SVsym-34 (SVsym for short) (stiff) [69]. These forces predict a significant difference in the parameter L at saturation, being 34 MeV for SVbas and 81 MeV for SVsym, with rather similar saturation values of J, 30 and 34 MeV, respectively. The

distinct difference in the rate of change of the symmetry energy with density as calculated with the SVbas and SVsym Skyrme forces is illustrated in Figure 3.

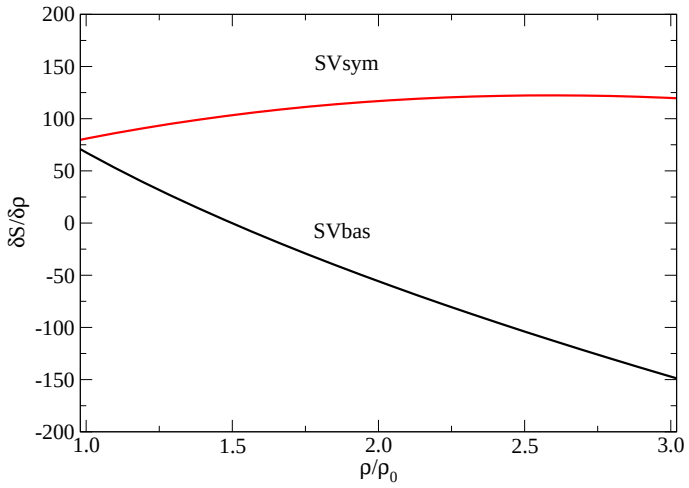

Figure 3. Derivative of symmetry energy with respect to density vs. total density normalized to ρ_0 as calculated with the SVbas and SVsym Skyrme forces. The density scale along the x-axis is the same as that along the y-axis in the top panels of in Figure 4.

The maximum total particle number density ρ_{max}/ρ_0 and related n-p asymmetry $\delta = (\rho_n - \rho_p)/(\rho_n + \rho_p)$ as a function of beam energy are illustrated in Figure 4 for the case of $^{212-208}$Pb collisions at beam energy 200–800 MeV/nucleon. The maximum total density does not exceed 2.5–3.0 ρ_0 and there is only marginal sensitivity of ρ_{max}/ρ_0 to density dependence of symmetry energy (top panels). The n-p asymmetry δ shows almost beam energy independent difference between predictions of SVbas and SVsym models (bottom panels). The SVbas model indicates a minor gain in asymmetry above the experimental value (blue dashed curves) while SVsym never reaches it. Therefore, a slight preference might be given to the soft SVbas model. Interestingly, the simulations revealed a significant role of the Coulomb interaction causing a substantial decrease in δ with respect to the experimental value [67]. The Coulomb effect cannot be switched off in the real world and must be taken into account in interpretation of data.

Nuclear symmetry energy and its density dependence are important in all density regimes, from supernovae at low densities, neutron-rich nuclei around saturation density and NS at several times the saturation value [63]. As already mentioned above, it is often argued that HIC provide the only terrestrial laboratory to study this density dependence using transport models. What is overlooked is that the structure of the matter created at HIC and that in the cores of NS are fundamentally different. In the near-symmetric systems in HIC only strong interaction acts in contrast with the highly asymmetric matter in NS both strong and weak interactions take place. It follows that particle composition and processes are present in NS, and, consequently, different EoS (for details see [21]) governs NS physics. On the technical side, the one term Taylor expansions used to extract density dependence of the symmetry energy are valid only close to saturation and are inadequate at higher density, definitely at several times nuclear saturation density (see Section 2.3). In addition, there is a difference in temperature and (mostly unknown) density dependence on typical lifetimes of strong and weak interactions [70]. Thus, we conclude that EoSs constructed on the basis of HIC data do not apply to NS.

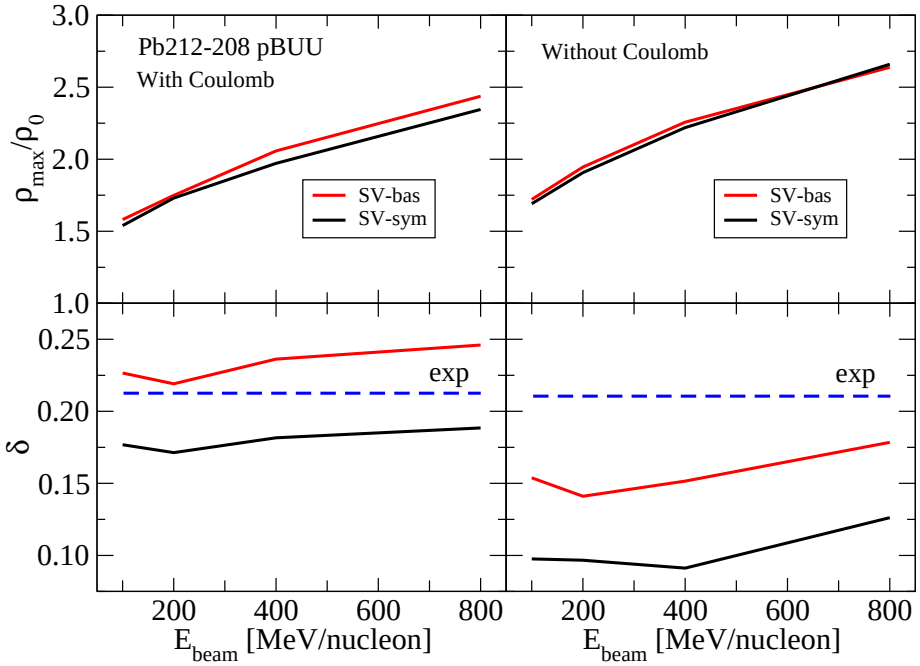

Figure 4. Maximum normalized particle number density (top panels) and n-p asymmetries δ (bottom panels) as a function of beam energy in the pBUU simulation for the SVbas (red) and SVsym (black) Skyrme symmetry energy models. Left and right panels: the results obtained with and without Coulomb interactions, respectively. For more explanation, see text and [66–68].

3.3. Neutron Skin Thickness

Neutron-heavy nuclei typically have non-uniform proton and neutron distributions with a neutron-rich outer layer, the neutron skin. A strong correlation between the neutron skin thickness and the rate of change in symmetry energy with increasing density (L) was found [71–73]. Using nuclear models sensitive to the density dependence of S can provide predictions of neutron skin, while experiments, in turn, provide information on L.

Figure 5 shows data on the neutron skin of the only two stable double-magic nuclei with a significant neutron excess in the entire nuclear chart, ^{48}Ca and ^{208}Pb, and their weighted average obtained with hadronic probes. By contrast, a purely electroweak determination of the neutron skin from measurement of parity-violation asymmetry A_{PV} in the scattering of longitudinally polarized electrons from an unpolarized target, first used by Donnelly et al. [74], was made at the Jefferson Laboratory, with results ^{48}Ca 0.121 $\pm$ 0.026 (exp) $\pm$ 0.024 (model) fm (CREX) [75]) and ^{208}Pb 0.283 $\pm$ 0.071 fm (PREX) [76]). Not shown is the recent measurement at LHC of the neutron skin in ^{208}Pb, 0.217 $\pm$ 0.058 fm, inferred from particle distributions and their collective flow in ultra-relativistic ^{208}Pb + ^{208}Pb collisions, mediated by interactions of gluons. We see that the CREX result is consistent with the weighted mean range of the hadronic experiments. The PREX value deviates considerably, whereas the LHC results, while somewhat high, are more consistent.

The goal of theory is to reproduce simultaneously the PREX and CREX results and global nuclear properties across the nuclear chart. Among the many calculations, Reed et al. [73], taking only the PREX data and using a special version of relativistic mean field models, obtained J, and L being $J = (38.1 \pm 4.7)$ MeV and $L = (106 \pm 37)$ MeV not consistent with all other available data (see Figure 6). Various other approaches such as nuclear energy density functional theory [77], other relativistic mean field models [78] and Bayesian analysis [79] have been employed without notable success in the interpretation of the CREX and PREX results, and the discussion continues.

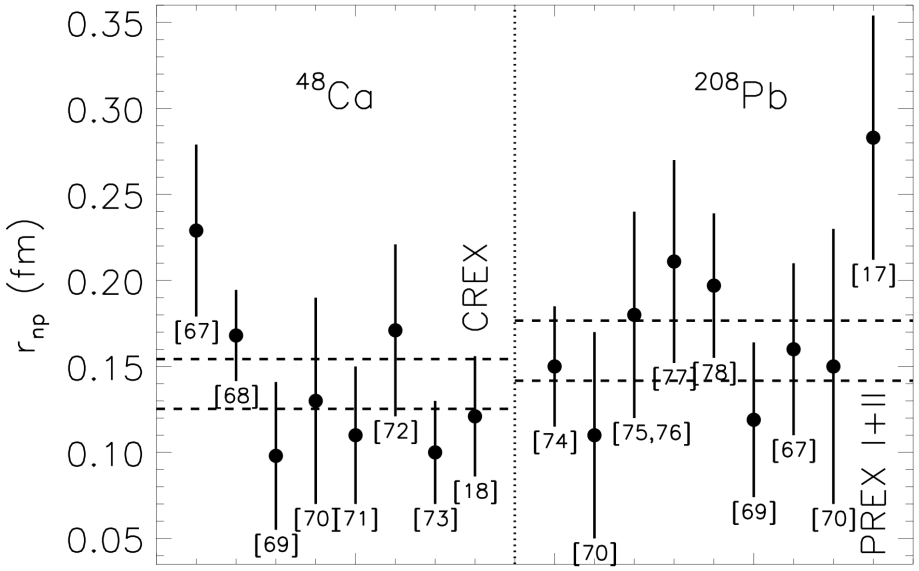

Figure 5. Neutron skin measurement with 68% confidence intervals and related citations. Horizontal dashed lines indicate ±1 standard deviations from the weighted means of experiments other than CREX or PREX I+II. The figure was taken from ref. [80] where the original references, under numbers [17,18,70–78], can be found. Others can be found in refs. [67–69].

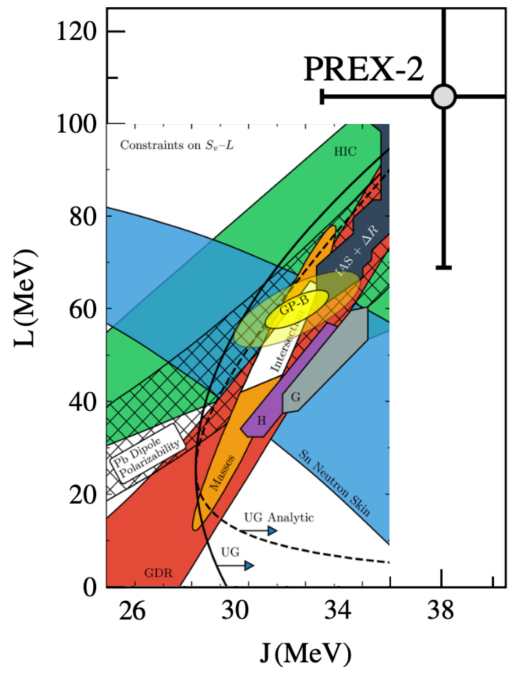

Figure 6. Constraints on the J–L correlation obtained from a variety of experimental and theoretical approaches. The figure was taken from ref. [73] to illustrate the tension with the recent PREX-II result.

3.4. Symmetry Energy Constraints from Combined Terrestrial and Astrophysical Data

The advent of new telescopes and gravitational wave (GW) detection systems has led to an increasing amount of data on cold and warm NS, supernovae and, more recently, GW. Two more quantities, the tidal deformation $\Lambda_{1.4}$ and the radius $R_{1.4}$ of 1.4 $M_\odot$ NS, have been added to the traditional maximum mass and radius of cold NS as variables required to test the validity of theoretical models. On the terrestrial side, the obligatory E_0 and ρ_0 have been complemented with dipole polarizability α_D [81,82], isobaric analog states [83–85], pygmy resonances [86,87], polarized proton elastic scattering [88], theoretical

PNM properties at low densities and temperatures (unitary gas) and related data on cold atoms [89]. It remains to be seen how much direct evidence regarding symmetry energy can be obtained from these new approaches.

There have been comprehensive reviews of methods and results covering symmetry energy and its density dependence studies based on the data, experiments and observations [33,35]. In this section, we mention only several recent works, some utilizing GW data, illustrative of the increasing diversity of the search for the density dependence of symmetry energy.

The vibration mode of the core–crust interface in neutron star binaries is sensitive to the symmetry energy profile of the dense matter in the NS core, as investigated by Neill et al. ([90] and the refs. therein). It was shown that the vibration triggers a resonant flare, Bayesian analysis reveals that coincident timing of the flare and GW signal during binary NS in spiral may yield new constraints on properties of the symmetry energy, comparable to those obtained from terrestrial nuclear experiments (see Figure 3 in [91]).

The possibility of constraining L using dynamics of GW emission and dynamical mass ejection in the post-merger phase of a binary neutron coalescence was studied by Most and Raithel [92]. Neutron star merger simulations in full general relativity indicated that post-merger dynamics and GW emission are insensitive to L, but the dynamical mass ejecta exhibit weak sensitivity to L, with large values of L tending to enhance ejecta. Such a correlation may be useful when the real post–merger GW signal is observed.

Providencia et al. [93] studied hyperonic stars in the framework of a relativistic mean field approach [94] in order to constrain the density dependence of symmetry energy. The effects of hyperon presence in the core on NS radius, the direct nucleonic and hyperonic URCA (DU) processes and the cooling of accreting NS were investigated. Correlations between L, the onset density of DU cooling process and hyperonic single-particle potentials were found. It was also shown that the electronic DU process is affected by hyperons only if the slope of the symmetry energy L is less than 70 MeV. Boukari and Rahbi [95] used the quark—meson–coupling–Bogoliubov model which includes u, d and s quarks to investigate effects of the slope of symmetry energy on the structure and properties of NS. They concluded that the improved model is in accordance with GW170817 observations and that the constrained symmetry energy does not allow for nucleonic direct URCA processes inside neutron stars or for hyperon nucleate inside neutron stars.

The possible existence of quark and/or hybrid NS stars with a quark core has been discussed in the literature for many decades. A phase transition from a low–density hadronic phase to a high–density quark phase on different scales, NS, HIC at ultra–high beam energy and early universe, was originally proposed in late 1970's and early 1980's [96–99]. More recently, hadron and quark phases and their onset and mixing in NS (see e.g., [38,100–119]) have been of interest despite no observational evidence having been found.

The quantities expected to be sensitive to the symmetry energy and its density dependence are the hadron–quark phase transition and its properties. Employing astrophysical data to constrain predictions of the hadron–quark transition in NS has been quite frequent in recent years. For example, Miao et al. [120], using a quark-mean-field model, found a strong correlation between the symmetry energy slope L and the properties of the hadron–quark phase transition. Limits on the maximum mass of NS, radius of 1.4 $M_{\odot}$ mass stars and the strength and density dependence of the hadron–quark phase transition were set. Liu et al. [116] investigated properties of the symmetry energy using a hybrid star with the hadron–quark phase transition and reached a similar conclusion, finding that the radii and tidal deformabilities of hybrid stars constrain mostly the density dependence of symmetry energy while the observed maximum masses of hybrid stars constrain mostly the EoSs of symmetric nuclear and quark matter.

A recent review by Aryal et al. [121] provides a comprehensive discussion of how different sets of conditions describing matter in NS and their mergers relate to those when the first-order hadron–quark transition and its eventual change to crossover takes place in HIC at ultra-high beam energies. The QCD phase diagram and the effect of charge,

isospin and strangeness on the critical end point (CEP), the end of a hadron–quark phase equilibrium curve, are also discussed.

The outcome of this review, based on the chiral mean field (CMF) model [122], makes a distinction between the HIC scenario (isospin symmetric, large charge fraction and low strangeness) and NS (isospin asymmetric, low charge fraction and high strangeness). In the latter scenario, the confinement transition comes at a lower baryon chemical potential, extends to higher temperature and presents a distinguished CEP signal. Such a prediction is interesting, as it is thought that strong first-order phase transitions can leave signals in the post–merger part of GW signals from NS mergers [123]. A more recent review by Pandav et al. [124] complements [121], includes information on the status of the experimental search for the critical point in HIC and comments on the physical implications of the data compared with theory (see section 2 of [124]).

The Adelaide–Saclay version of the quark–meson coupling model (QMC) [125–129] has been applied to both atomic nuclei and nuclear matter. A recent study [130], aiming to take account of the correlations between values the three nuclear matter parameters, searched a 3D mesh with "coordinates" (ρ_0, E_0, J) with ranges of ρ_0 0.14–17 fm^{-3}, E_0 from -15 to -18 MeV and J between 27 and 36 MeV. Each matrix point chosen determines the coupling constants of the model and hence allows for the calculation of a variety of nuclear matter and NS properties. When these were compared with expected empirical and observational values, only two sets, $\rho_0 = 0.16$ $E_0 = -15$ or -16 MeV and $J = 31$ MeV, satisfied all the data. A clear success of the model was that the coupling constants associated with the successful sets $9.5 \leq G_\sigma \leq 10.0$ fm^2, $5.8 \leq G_\omega \leq 6.1$ fm^2 and $3.35 \leq G_\rho \leq 3.45$ fm^2 were entirely consistent with the best-fit values when the model was applied to atomic nuclei [131,132].

Adam et al. used the generalized Skyrme model [133,134] (not to be confused with the model familiar in nuclear energy density functional) to calculate the symmetry energy and its density dependence in nuclear matter. The binding energy of skyrmion crystals, the building blocks of the model, is sensitive to the isospin degrees of freedom. This mathematical model allows the investigation of non-perturbative features of strongly interacting matter at all scales, from single baryons and nuclei to NS. The symmetry energy and relative fractions of neutrons, protons, electrons and muons in β-equilibrated asymmetric nuclear matter was calculated as a function of the baryon number density, and the best values obtained for SNM parameters at saturation were $S_0 = 31.9$ MeV, $L = 46.4$ MeV and $\rho_0 = 0.22$ fm^{-3}. It is interesting that this very different concept of nuclear structure produces results comparable with traditional values (although with a slightly higher ρ_0).

4. Conclusions and Outlook

Following a general introduction to the role of symmetry and its breaking in nature, our work has focused on the concept of charge symmetry and its breaking at the nuclear level.

The phenomenology of symmetry energy has been discussed starting with introduction of the concept of nuclear matter. It is argued that the two extreme forms of INM, namely the fully excited state (PNM) and the asymmetric ground state (SNM) of nuclear matter, can be interpreted as an example of spontaneous charge symmetry breaking by the strong force. In this context, the symmetry energy can be perceived as a measure of the energy released during this process. It is essential to obtain as accurate as possible information on the properties of symmetry energy.

An extensive search for the effects of symmetry energy and its density dependence in a wide variety of systems, including mirror nuclei, heavy-ion collisions, neutron skin, cold NS, products of NS coalescence and skyrmion crystals, employing many theoretical models, has been reviewed. Two main conclusions emerged:

(i) It is interesting that the most basic properties of nuclear matter, a hypothetical medium not existing in nature and introduced to physics in 1930's as a highly simplified testing ground of nuclear models, are still in use despite the mainly classical rudimentary assumptions leading to their derivation (see Sections 2.2 and 2.3). The current range of the

value of symmetry energy S at saturation density, $S_0 = J$, falls between 26 and 35 MeV, with the most probable value around 30–32 MeV. This differs little from early analysis based on the simple semi-empirical mass formula [21]. The rather small variation in the value of J, almost independent of the nuclear system used for its extraction, may be related to its origin in the exchange of u and d quarks (see Section 2.1). The value of the slope L is extracted from Taylor expansions of binding energy of nuclei in LDM in terms of n-p asymmetry δ and the density deviations from the saturation value ε. It is a common practice to utilize only first terms of these expansions, which inevitably becomes inadequate at higher densities and/or particle density asymmetries (see Section 2.3). This may be one of the reasons why there is no generally accepted result available and extracted values of L range from about 20 to 100+ MeV (see Figure 6). Note that the value of L found by Myers and Swiatecky in 1969 [27] is 123 MeV for J = 28 MeV, not fully inconsistent with current limits.

(ii) The choice of nuclear models and methods plays an important role in any attemps to determine the symmetry energy density dependence. Models of different physical scenarios have varying sensitivities to the effect of symmetry energy compared to other factors, not always considered at an adequate level. Highly asymmetric systems, such NSs, are favored over close-to-symmetric ones, such as HIC or supernovae. Moreover, the theoretical accuracy of a model, which is admittedly not easy to estimate, is hardly ever explicitly included in the uncertainty of a calculated quantity. It follows that, as discussed in this work, we currently have as many mutually inconsistent L values as we have models, illustrating the diversity in model construction and application. The models and methods are not focused enough to produce a coherent and credible background for the overall assessment of the symmetry energy and its properties.

To gain perspectives for any future investigations into symmetry energy and its density dependence in nuclear matter and finite nuclear systems, it is essential to better understand and minimize the effects of model dependencies. Furthermore, reducing errors of the data used to fit numerous variable model parameters is desirable. It should also be recognized that while the symmetry energy is a significant factor in nuclear physics, charge symmetry and its breaking are only some of the many poorly known factors playing roles in the nuclear force. Major advancements in the determination of the properties of symmetry energy (on the nucleon level) are unlikely to occur until a more fundamental understanding of the nuclear force itself is achieved.

Funding: This research received no external funding.

Data Availability Statement: Not applicable.

Conflicts of Interest: The author declares no conflict of interest.

References

1. Noether, E. Invariante Variationsprobleme. In *Gesammelte Abhandlungen-Collected Papers*; Springer: Berlin/Heidelberg, Germany, 1983; pp. 235–257.
2. Noether, E. Invariant variation problems. *Transp. Theory Stat. Phys.* **1971**, *1*, 186–207. [CrossRef]
3. Kosmann, Y.; Schwarzbach, B.E. *The Noether Theorems: Invariance and Conservation Laws in the Twentieth Century*; Springer: New York, NY, USA, 2011; ISBN 9780387878683. [CrossRef]
4. Brading, K.A. Which symmetry? Noether, Weyl, and conservation of electric charge. *Stud. Hist. Philos. Sci. Part B Stud. Hist. Philos. Mod. Phys.* **2002**, *33*, 3–22. [CrossRef]
5. Greaves, H.; Thomas, T. On the CPT theorem. *Stud. Hist. Philos. Sci. Part B Stud. Hist. Philos. Mod. Phys.* **2014**, *45*, 46–65. [CrossRef]
6. Swanson, N. Deciphering the algebraic CPT theorem. *Stud. Hist. Philos. Sci. Part B Stud. Hist. Philos. Mod. Phys.* **2019**, *68*, 106–125. [CrossRef]
7. Brading, K.; Castellani, E.; Teh, N. Symmetry and Symetry Braking. In *The Stanford Encyclopedia of Philosophy*, Fall 2023 ed.; Zalta, E.N., Nodelman, U., Eds.; Metaphysics Research Lab, Stanford University: Stanford, CA, USA, 2003. Available online: https://plato.stanford.edu/archives/fall2023/entries/symmetry-breaking/ (accessed on 21 April 2024).
8. Higgs, P.W. Broken Symmetries and the Masses of Gauge Bosons. *Phys. Rev. Lett.* **1964**, *13*, 508–509. [CrossRef]
9. Heisenberg, W. Über Den Bau der Atomkerne. I. *Z. Für. Phys.* **1932**, *77*, 1–11. [CrossRef]

10. Wigner, E. On the Consequences of the Symmetry of the Nuclear Hamiltonian on the Spectroscopy of Nuclei. *Phys. Rev.* **1937**, *51*, 106–119. [CrossRef]
11. Yang, C.N.; Mills, R.L. Conservation of Isotopic Spin and Isotopic Gauge Invariance. *Phys. Rev.* **1954**, *96*, 191–195. [CrossRef]
12. Epelbaum, E.; Hammer, H.-W. Meißner, U.-G. Modern theory of nuclear forces. *Rev. Mod. Phys.* **2009**, *81*, 1773–1825. [CrossRef]
13. Machleidt, R.; Entem, D.R. Nuclear forces from chiral EFT: The unfinished business. *J. Phys. G Nucl. Part Phys.* **2010**, *37*, 064041. [CrossRef]
14. Machleidt, R.; Entem, D.R. Chiral effective field theory and nuclear forces. *Phys. Rep.* **2011**, *503*, 1–75. [CrossRef]
15. Holt, J.W.; Kaiser, N. Equation of state of nuclear and neutron matter at third-order in perturbation theory from chiral effective field theory. *Phys. Rev. C* **2017**, *95*, 034326. [CrossRef]
16. Sammarruca, F. The Symmetry Energy: Current Status of Ab Initio Predictions vs. Empirical Constraints. *Symmetry* **2023**, *15*, 450. [CrossRef]
17. Gamow, G. Mass defect curve and nuclear constitution. *Proc. R. Soc. London Ser. A Contain. Pap. Math. Phys. Character* **1930**, *126*, 632–644. [CrossRef]
18. Weizsacker, C.F.v. Zur Theorie der Kernmassen. *Z. Für Phys.* **1935**, *96*, 431–458. [CrossRef]
19. Bethe, H.A.; Bacher, R.F. Nuclear Physics A. Stationary States of Nuclei. *Rev. Mod. Phys.* **1936**, *8*, 82–229. [CrossRef]
20. Kirson, M.W. Mutual influence of terms in a semi-empirical mass formula. *Nucl. Phys. A* **2008**, *798*, 29–60. [CrossRef]
21. Stone, J.R. Nuclear Physics and Astrophysics Constraints on the High Density Matter Equation of State. *Universe* **2021**, *7*, 257. [CrossRef]
22. Bethe, H.A. Theory of Nuclear Matter. *Annu. Rev. Nucl. Sci.* **1971**, *21*, 93–244. [CrossRef]
23. Hofstadter, R. Electron scattering and nuclear structure. *Rev. Mod. Phys.* **1956**, *28*, 214–254. [CrossRef]
24. Hofstadter, R.; Bumiller, F.; Yearian, M.R. Electromagnetic structure of the proton and neutron. *Rev. Mod. Phys.* **1958**, *30*, 482–497. [CrossRef]
25. Miller, G.; Nefkens, B.; Šlaus, I. Charge symmetry, quarks and mesons. *Phys. Rep.* **1990**, *194*, 1–116. [CrossRef]
26. Myers, W.D.; Swiatecki, W.J. Nuclear masses and deformations. *Nucl. Phys.* **1966**, *81*, 1–60. [CrossRef]
27. Myers, W.D.; Swiatecki, W.J. Average nuclear properties. *Ann. Phys.* **1969**, *55*, 395–505. [CrossRef]
28. Myers, W.D.; Switecki, W.J. The nuclear droplet model for arbitrary shapes. *Ann. Phys.* **1974**, *84*, 186–210. [CrossRef]
29. Moller, P.; Nix, J.R.; Myers, W.D.; Swiatecki, W.J. Nuclear ground-state masses and deformations. *At. Data Nucl. Data Tables* **1995**, *59*, 185–381. Available online: http://www.sciencedirect.com/science/article/pii/S0092640X85710029 (accessed on 1 January 2024). [CrossRef]
30. Möller, P.; Myers, W.D.; Sagawa, H.; Yoshida, S. New Finite-Range Droplet Mass Model and Equation-of-State Parameters. *Phys. Rev. Lett.* **2012**, *108*, 052501. [CrossRef]
31. Möller, P.; Sierk, A.J.; Ichikawa, T.; Sagawa, H. Nuclear ground-state masses and deformations: FRDM(2012). *At. Data Nucl. Data Tables* **2016**, *109–110*, 1–204. Available online: http://www.sciencedirect.com/science/article/pii/S0092640X1600005X (accessed on 10 January 2024). [CrossRef]
32. Baldo, M.; Burgio, G.F. Properties of the nuclear medium. *Rep. Prog. Phys.* **2012**, *75*, 026301. [CrossRef]
33. Tsang, M.B.; Stone, J.R.; Camera, F.; Danielewicz, P.; Gandolfi, S.; Hebeler, K.; Horowitz, C.J.; Lee, J.; Lynch, W.G.; Kohley, Z.; et al. Constraints on the symmetry energy and neutron skins from experiments and theory. *Phys. Rev. C* **2012**, *86*, 015803. [CrossRef]
34. Li, B.-A.; Ramos, À.; Verde, G.; Vidaña, I. Topical issue on nuclear symmetry energy. *Eur. Phys. J. A* **2014**, *50*, 9. [CrossRef]
35. Horowitz, C.J.; Brown, E.F.; Kim, Y.; Lynch, W.G.; Michaels, R.; Ono, A.; Piekarewicz, J.; Tsang, M.B.; Wolter, H.H. A way forward in the study of the symmetry energy: Experiment, theory, and observation. *J. Phys. Nucl. Part. Phys.* **2014**, *41*, 093001. [CrossRef]
36. Baldo, M.; Burgio, G. The nuclear symmetry energy. *Prog. Part. Nucl. Phys.* **2016**, *91*, 203–258. [CrossRef]
37. Bednarek, I.; Sładkowski, J.; Syska, J. Forms of the Symmetry Energy Relevant to Neutron Stars. *Symmetry* **2020**, *12*, 898. [CrossRef]
38. Li, B.-A.; Cai, B.-J.; Xie, W.-J.; Zhang, N.-B. Progress in Constraining Nuclear Symmetry Energy Using Neutron Star Observables Since GW170817. *Universe* **2021**, *7*, 182. [CrossRef]
39. Okamoto, K. Coulomb energy of He^3 and possible charge asymmetry of nuclear forces. *Phys. Lett.* **1964**, *11*, 150–153. [CrossRef]
40. Nolen, J.A.; Schiffer, J.P. Coulomb Energies. *Annu. Rev. Nucl. Sci.* **1969**, *19*, 471–526. [CrossRef]
41. Negele, J. The ^{41}Sc-^{41}Ca Coulomb energy difference. *Nucl. Phys. A* **1971**, *165*, 305–326. [CrossRef]
42. Wilkinson, D. The Nolen-Schiffer anomaly and the conserved vector current. *Phys. Lett. B* **1974**, *48*, 407–409. [CrossRef]
43. Suzuki, T.; Sagawa, H.; Arima, A. Effects of valence nucleon orbits and charge symmetry breaking interaction on the Nolen-Schiffer anomally of mirror nuclei. *Nucl. Phys. A* **1992**, *536*, 141–158. [CrossRef]
44. Shahnas, M.H. Nolen-Schiffer anomaly of mirror nuclei and charge symmetry breaking in nuclear interactions. *Phys. Rev. C* **1994**, *50*, 2346–2350. [CrossRef]
45. Cardarelli, F.; Piekarewicz, J. The Okamoto-Nolen-Schiffer anomaly without p-ω mixing. *Nucl. Phys. A* **1997**, *612*, 429–448. [CrossRef]
46. Menezes, D.P.; Avancini, S.S.; Vasconcellos, C.Z.;Z Razeira, M. δ meson effects in the Nolen-Schiffer anomaly. *Eur. Phys. J. A* **2009**, *42*, 97. [CrossRef]

47. Li, H.H.; Yuan, Q.; Li, J.G.; Xie, M.R.; Zhang, S.; Zhang, Y.H.; Xu, X.X.; Michel, N.; Xu, F.R.; Zuo, W. Investigation of isospin-symmetry breaking in mirror energy difference and nuclear mass with ab initio calculations. *Phys. Rev. C* **2023**, *107*, 014302. [CrossRef]
48. Saito, K.; Thomas, A. The Nolen-Schiffer anomaly and isospin symmetry breaking in nuclear matter. *Phys. Lett. B* **1994**, *335*, 17–23. [CrossRef]
49. Sagawa, H.; Naito, T.; Roca-Maza, X.; Hatsuda, T. QCD-based charge symmetry breaking interaction and the Okamoto-Nolen-Schiffer anomaly. *Phys. Rev. C* **2024**, *109*, l011302. [CrossRef]
50. Danielewicz, P.; Lacey, R.; Lynch, W.G. Determination of the Equation of State of Dense Matter. *Science* **2002**, *298*, 1592–1596. [CrossRef] [PubMed]
51. Tsang, M.B.; Liu, T.X.; Shi, L.; Danielewicz, P.; Gelbke, C.K.; Liu, X.D.; Lynch, W.G.; Tan, W.P.; Verde, G.; Wagner, A.; et al. Isospin Diffusion and the Nuclear Symmetry Energy in Heavy Ion Reactions. *Phys. Rev. Lett.* **2004**, *92*, 062701. [CrossRef] [PubMed]
52. Famiano, M.A.; Liu, T.; Lynch, W.G.; Mocko, M.; Rogers, A.M.; Tsang, M.B.; Wallace, M.S.; Charity, R.J.; Komarov, S.; Sarantites, D.G.; et al. Neutron and Proton Transverse Emission Ratio Measurements and the Density Dependence of the Asymmetry Term of the Nuclear Equation of State. *Phys. Rev. Lett.* **2006**, *97*, 052701. [CrossRef]
53. Liu, T.X.; Lynch, W.G.; Tsang, M.B.; Liu, X.D.; Shomin, R.; Tan, W.P.; Verde, G.; Wagner, A.; Xi, H.F.; Xu, H.S. et al. Isospin diffusion observables in heavy-ion reactions. *Phys. Rev. C* **2007**, *76*, 034603. [CrossRef]
54. Xiao, Z.; Li, B.-A.; Chen, L.-W.; Yong, G.-C.; Zhang, M. Circumstantial Evidence for a Soft Nuclear Symmetry Energy at Suprasaturation Densities. *Phys. Rev. Lett.* **2009**, *102*, 062502. [CrossRef]
55. Feng, Z.-Q.; Jin, G.-M. Probing high-density behavior of symmetry energy from pion emission in heavy-ion collisions. *Phys. Lett. B* **2010**, *683*, 140–144. [CrossRef]
56. Xie, W.-J.; Su, J.; Zhu, L.; Zhang, F.-S. Symmetry energy and pion production in the Boltzmann–Langevin approach. *Phys. Lett. B* **2013**, *718*, 1510–1514. [CrossRef]
57. Jhang, G.; Estee, J.; Barney, J.; Cerizza, G.; Kaneko, M.; Lee, J.; Lynch, W.; Isobe, T.; Kurata-Nishimura, M.; Murakami, T.; et al. Symmetry energy investigation with pion production from Sn+Sn systems. *Phys. Lett. B* **2021**, *813*, 136016. [CrossRef]
58. Cozma, M.D.; Tsang, M.B. In-medium $\Delta(1232)$ potential, pion production in heavy-ion collisions and the symmetry energy. *Eur. Phys. J. A* **2021**, *57*, 11. [CrossRef]
59. Lynch, W.; Tsang, M. Decoding the density dependence of the nuclear symmetry energy. *Phys. Lett. B* **2022**, *830*, 137098. [CrossRef]
60. Bertsch, G.F.; Das Gupta, S. A guide to microscopic models for intermediate energy heavy ion collisions. *Phys. Rep.* **1988**, *160*, 189–233. [CrossRef]
61. Danielewicz, P. Determination of the mean-field momentum-dependence using elliptic flow. *Nucl. Phys. A* **2000**, *673*, 375–410. [CrossRef]
62. Aichelin, J. Heavy systems at intermediate energies in the Boltzmann-Uehling-Uhlenbeck approach. *Phys. Rev. C* **1986**, *33*, 537–548. [CrossRef] [PubMed]
63. Wolter, H.H. The nuclear symmetry energy in heavy ion collisions. *Phys. Part. Nucl.* **2015**, *46*, 781–785. [CrossRef]
64. Xu, J.; Chen, L.-W.; Tsang, M.B.; Wolter, H.; Zhang, Y.-X.; Aichelin, J.; Colonna, M.; Cozma, D.; Danielewicz, P.; Feng, Z.-Q.; et al. Understanding transport simulations of heavy-ion collisions at 100A and 400A MeV: Comparison of heavy-ion transport codes under controlled conditions. *Phys. Rev. C* **2016**, *93*, 044609. [CrossRef]
65. Wolter, H.; Colonna, M.; Cozma, D.; Danielewicz, P.; Ko, C.M.; Kumar, R.; Ono, A.; Tsang, M.B.; Xu, J.; Zhang, Y.-X. et al. Transport model comparison studies of intermediate-energy heavy-ion collisions. *Prog. Part. Nucl. Phys.* **2022**, *125*, 103962. [CrossRef]
66. Stone, J.R.; Danielewicz, P.; Iwata, Y. Proton and neutron density distributions at supranormal density in low- and medium-energy heavy-ion collisions. *Phys. Rev. C* **2017**, *96*, 014612. [CrossRef]
67. Stone, J.; Danielewicz, P.; Iwata, Y. Coulomb effects in low- and medium-energy heavy-ion collisions. *Phys. Lett. B* **2022**, *826*, 136915. [CrossRef]
68. Stone, J.R.; Danielewicz, P.; Iwata, Y. Proton and neutron density distributions at supranormal density in low- and medium-energy heavy-ion collisions. II. Central Pb + Pb collisions. *Phys. Rev. C* **2024**, *109*, 044603. [CrossRef]
69. Klüepfel, P.; Reinhard, P.-G.; Bürvenich, T.J.; Maruhn, J.A. Variations on a theme by Skyrme: A systematic study of adjustments of model parameters. *Phys. Rev. C* **2009**, *79*, 034310. [CrossRef]
70. Gourgoulhon, E.; Haensel, P.; Gondek, D. Maximum mass instability of neutron stars and weak interaction processes in dense matter. *Astron Astrophys J.* **1995**, *294*, 747–756.
71. Horowitz, C.J.; Piekarewicz, J. Neutron Star Structure and the Neutron Radius of ^{208}Pb. *Phys. Rev. Lett.* **2001**, *86* 5647–5650. [CrossRef]
72. Thiel, M.; Sfienti, C.; Piekarewicz, J.; Horowitz, C.J.; Vanderhaeghen, M. Neutron skins of atomic nuclei: Per aspera ad astra. *J. Phys. G Nucl. Part. Phys.* **2019**, *46*, 093003. [CrossRef]
73. Reed, B.T.; Fattoyev, F.; Horowitz, C.; Piekarewicz, J. Implications of PREX-2 on the Equation of State of Neutron-Rich Matter. *Phys. Rev. Lett.* **2021**, *126*, 172503. [CrossRef]

74. Donnelly, T.; Dubach, J.; Sick, I. Isospin dependences in parity-violating electron scattering. *Nucl. Phys. A* **1989**, *503*, 589–631. [CrossRef]
75. Adhikari, D.; Albataineh, H.; Androic, D.; Aniol, K.; Armstrong, D.; Averett, T.; Ayerbe Gayoso, C.; Barcus, S.; Bellini, V.; Beminiwattha, R.; et al. Precision Determination of the Neutral Weak Form Factor of ^{48}Ca. *Phys. Rev. Lett.* **2022**, *129*, 042501. [CrossRef] [PubMed]
76. Adhikari, D.; Albataineh, H.; Androic, D.; Aniol, K.; Armstrong, D.; Averett, T.; Ayerbe Gayoso, C.; Barcus, S.; Bellini, V.; Beminiwattha, R.; et al. Accurate Determination of the Neutron Skin Thickness of ^{208}Pb through Parity-Violation in Electron Scattering. *Phys. Rev. Lett.* **2021**, *126*, 172502. [CrossRef] [PubMed]
77. Reinhard, P.-G.; Roca-Maza, X.; Nazarewicz, W. Combined Theoretical Analysis of the Parity-Violating Asymmetry for ^{48}Ca and ^{208}Pb. *Phys. Rev. Lett.* **2022**, *129*, 232501. [CrossRef]
78. Miyatsu, T.; Cheoun, M.-K.; Kim, K.; Saito, K. Can the PREX-2 and CREX results be understood by relativistic mean-field models with the astrophysical constraints? *Phys. Lett. B* **2023**, *843*, 138013. [CrossRef]
79. Zhang, Z.; Chen, L.-W. Bayesian inference of the symmetry energy and the neutron skin in ^{48}Ca and ^{208}Pb from CREX and PREX-2. *Phys. Rev. C* **2023**, *108*, 024317. [CrossRef]
80. Lattimer, J.M. Constraints on Nuclear Symmetry Energy Parameters. *Particles* **2023**, *6*, 30–56. [CrossRef]
81. Roca-Maza, X.; Brenna, M.; Colò, G.; Centelles, M.; Viñas, X.; Agrawal, B.K.; Paar, N.; Vretenar, D.; Piekarewicz, J. Electric dipole polarizability and its application for neutron skin. *Phys. Rev. C* **2013**, *88*, 024316. [CrossRef]
82. Birkhan, J.; Miorelli, M.; Bacca, S.; Bassauer, S.; Bertulani, C.; Hagen, G.; Matsubara, H.; von Neumann-Cosel, P.; Papenbrock, T.; Pietralla, N.; et al. Electric Dipole Polarizability of ^{48}Ca and Implications for the Neutron Skin. *Phys. Rev. Lett.* **2017**, *118*, 252501. [CrossRef] [PubMed]
83. Jänecke, J. On isobaric analogue states. *Nucl. Phys.* **1965**, *73*, 97–112. [CrossRef]
84. Danielewicz, P.; Lee, J. Symmetry energy II: Isobaric analog states. *Nucl. Phys. A* **2014**, *922*, 1–70. [CrossRef]
85. Roca-Maza, X.; Colò, G.; Sagawa, H. Nuclear Symmetry Energy and the Breaking of the Isospin Symmetry: How Do They Reconcile with Each Other? *Phys. Rev. Lett.* **2018**, *120*, 202501. [CrossRef] [PubMed]
86. Savran, D.; Aumann, T.; Zilges, A. Experimental studies of the Pygmy Dipole Resonance. *Prog. Part. Nucl. Phys.* **2013**, *70*, 210–245. [CrossRef]
87. Tsoneva, N.; Spieker, M.; Lenske, H.; Zilges, A. Fine structure of the pygmy quadrupole resonance in ^{112,114}Sn. *Nuclear Physics A* **2019**, *990*, 183–198. [CrossRef]
88. Zenihiro, J.; Sakaguchi, H.; Murakami, T.; Yosoi, M.; Yasuda, Y.; Terashima, S.; Iwao, Y.; Takeda, H.; Itoh, M.; Yoshida, H.P.; et al. Neutron density distributions of ^{204,206,208}Pb deduced via proton elastic scattering at $E_p = 295$ MeV. *Phys. Rev. C* **2010**, *82*, 044611. [CrossRef]
89. Vidaña, I. Low-Density Neutron Matter and the Unitary Limit. *Front. Phys.* **2021**, *9*. [CrossRef]
90. Neill, D.; Newton, W.G.; Tsang, D. Resonant shattering flares as multimessenger probes of the nuclear symmetry energy. *Mon. Not. R. Astron. Soc.* **2021**, *504*, 1129–1143. [CrossRef]
91. Neill, D.; Preston, R.; Newton, W.G.; Tsang, D. Constraining the Nuclear Symmetry Energy with Multimessenger Resonant Shattering Flares. *Phys. Rev. Lett.* **2023**, *130*, 112701. [CrossRef]
92. Most, E.R.; Raithel, C.A. Impact of the nuclear symmetry energy on the post-merger phase of a binary neutron star coalescence. *Phys. Rev. D* **2021**, *104*, 124012. [CrossRef]
93. Providência, C.; Fortin, M.; Pais, H.; Rabhi, A. Hyperonic Stars and the Nuclear Symmetry Energy. *Front. Astron. Space Sci.* **2019**, *6*, 13. [CrossRef]
94. Dutra, M.; Lourenço, O.; Avancini, S.S.; Carlson, B.V.; Delfino, A.; Menezes, D.P.; Providência, C.; Typel, S.; Stone, J.R. Relativistic mean–field hadronic models under nuclear matter constraints. *Phys. Rev. C* **2014**, *90*, 055203. [CrossRef]
95. Boukari, O.; Rabhi, A. Nuclear Symmetry Energy Effects on Neutron Star Properties within Bogoliubov-Quark–Meson-Coupling Model. *Symmetry* **2023**, *15*, 1742. [CrossRef]
96. Collins, J.C.; Perry, M.J. Superdense Matter: Neutrons or Asymptotically Free Quarks? *Phys. Rev. Lett.* **1975**, *34*, 1353–1356. [CrossRef]
97. Baym, G. Confinement of quarks in nuclear matter. *Phys. A Stat. Mech. Its Appl.* **1979**, *96*, 131–135. [CrossRef]
98. Olive, K.A. The stability of quark matter. *Phys. Lett. B* **1982**, *116*, 137–140. [CrossRef]
99. Witten, E. Cosmic separation of phases. *Phys. Rev. D* **1984**, *30*, 272–285. [CrossRef]
100. Weber, F. Quark matter in neutron stars. *J. Phys. G Nucl. Part Phys.* **1999**, *25*, R195–R229. [CrossRef]
101. Weber, F. Strange quark matter and compact stars. *Prog. Part. Nucl. Phys.* **2005**, *54*, 193–288. [CrossRef]
102. Alford, M.; Braby, M.; Paris, M.; Reddy, S. Hybrid Stars that Masquerade as Neutron Stars. *Astrophys. J.* **2005**, *629*, 969–978. [CrossRef]
103. Alford, M.G. Quark matter in neutron stars. *Nucl. Phys. A* **2009**, *830*, 385c–392c. [CrossRef]
104. Chu, P.-C.; Chen, L.-W. Quark matter symmetry energy and quark stars. *Astrophys. J.* **2013**, *780*, 135. [CrossRef]
105. Chen, L.-W. The symmetry energy in nucleon and quark matter. *arXiv* **2017**, arXiv:1708.04433. [CrossRef]
106. Lastowiecki, R.; Blaschke, D.; Fischer, T.; Klähn, T. Quark matter in high-mass neutron stars? *Phys. Part. Nucl.* **2015**, *46*, 843–845. [CrossRef]
107. Roark, J.; Dexheimer, V. Deconfinement phase transition in proto-neutron-star matter. *Phys. Rev. C* **2018**, *98*, 055805. [CrossRef]

108. Weber, F.; Farrell, D.; Spinella, W.M.; Malfatti, G.; Orsaria, M.G.; Contrera, G.A.; Maloney, I. Phases of hadron-quark matter in (proto) neutron stars. *Universe* **2019**, *5*, 169. [CrossRef]
109. Roark, J.; Du, X.; Constantinou, C.; Dexheimer, V.; Steiner, A.W.; Stone, J.R. Hyperons and quarks in proto-neutron stars. *MNRAS* **2019**, *486*, 5441–5447. [CrossRef]
110. Baym, G.; Furusawa, S.; Hatsuda, T.; Kojo, T.; Togashi, H. New neutron star equation of state with quark-hadron crossover. *Astrophys. J.* **2019**, *885*, 42. [CrossRef]
111. Spinella, W.M.; Weber, F.; Contrera, G.A.; Orsaria, M.G. *Discoveries at the Frontiers of Science*; Springer International Publishing: Cham, Switzerland, 2020; pp. 95–106. [CrossRef]
112. Annala, E.; Gorda, T.; Kurkela, A.; Nättilä, J.; Vuorinen, A. Evidence for quark-matter cores in massive neutron stars. *Nat. Phys.* **2020**, *16*, 907. [CrossRef]
113. Backes, B.C.T.; Marquezb, K.D.; Menezes, D.P. Effects of strong magnetic fields on the hadron-quark deconfinement transition. *Eur. Phys. J. A* **2021**, *57*, 229. [CrossRef]
114. Blaschke, D.; Cierniak, M. Studying the onset of deconfinement with multi-messenger astronomy of neutron stars. *Astron. Nachrichten* **2021**, *342*, 227–233. [CrossRef]
115. Kapusta, J.I.; Welle, T. Neutron stars with a crossover equation of state. *Phys. Rev. C* **2021**, *104*, l012801. [CrossRef]
116. Liu, H.; Xu, J.; Chu, P.-C. Symmetry energy effects on the properties of hybrid stars. *Phys. Rev. D* **2022**, *105*, 043015. [CrossRef]
117. Contrera, G.A.; Blaschke, D.; Carlomagno, J.P.; Grunfeld, A.G.; Liebing, S. Quark-nuclear hybrid equation of state for neutron stars under modern observational constraints. *Phys. Rev. C* **2022**, *105*, 045808. [CrossRef]
118. Kumar, A.; Thapa, V.B.; Sinha, M. Hybrid stars are compatible with recent astrophysical observations. *Phys. Rev. D* **2023**, *107*, 063024. [CrossRef]
119. Issifu, A.; da Silva, F.M.; Menezes, D.P. Hybrid stars built with density-dependent models. *Mon. Not. R. Astron. Soc.* **2023**, *525*, 5512–5519. [CrossRef]
120. Miao, Z.; Li, A.; Zhu, Z.; Han, S. Constraining Hadron-quark Phase Transition Parameters within the Quark-mean-field Model Using Multimessenger Observations of Neutron Stars. *Astrophys. J.* **2020**, *904*, 103. [CrossRef]
121. Aryal, K.; Constantinou, C.; Farias, R.L.S.; Dexheimer, V. The Effect of Charge, Isospin, and Strangeness in the QCD Phase Diagram Critical End Point. *Universe* **2021**, *7*, 454. [CrossRef]
122. Dexheimer, V.A.; Schramm, S. Novel approach to modeling hybrid stars. *Phys. Rev. C* **2010**, *81*, 045201. [CrossRef]
123. Most, E.R.; Papenfort, L.J.; Dexheimer, V.; Hanauske, M.; Schramm, S.; Stöcker, H.; Rezzolla, L. Signatures of Quark-Hadron Phase Transitions in General-Relativistic Neutron-Star Mergers. *Phys. Rev. Lett.* **2019**, *122*, 061101. [CrossRef]
124. Pandav, A.; Mallick, D.; Mohanty, B. Search for the QCD critical point in high energy nuclear collisions. *Prog. Part. Nucl. Phys.* **2022**, *125*, 103960. [CrossRef]
125. Guichon, P.A.M. A possible quark mechanism for the saturation of nuclear matter. *Phys. Lett. B* **1988**, *200*, 235. [CrossRef]
126. Guichon, P.A.M.; Saito, K.; Rodionov, E.N.; Thomas, A.W. The role of nucleon structure in finite nuclei. *Nucl. Phys. A* **1996**, *601*, 349. [CrossRef]
127. Guichon, P.A.M.; Thomas, A.W. Quark structure and nuclear effective forces. *Phys. Rev. Lett.* **2004**, *93*, 132502. [CrossRef]
128. Guichon, P.A.M.; Stone, J.R.; Thomas, A.W. Quark–Meson-Coupling (QMC) model for finite nuclei, nuclear matter and beyond. *Prog. Part. Nucl. Phys.* **2018**, *100*, 262–297. [CrossRef]
129. Stone, J.R.; Dexheimer, V.; Guichon, P.A.M.; Thomas, A.W.; Typel, S. Equation of state of hot dense hyperonic matter in the Quark-Meson-Coupling (QMC-A) model. *Mon. Not. R. Astron. Soc.* **2021**, *502*, 3476–3490. [CrossRef]
130. Stone, J.R.; Guichon, P.A.M.; Thomas, A.W. Nuclear Symmetry Energy and Hyperonic Stars in the QMC Model. *Front. Astron. Space Sci.* **2022**, *9*, 903007. [CrossRef]
131. Martinez, K.L.; Thomas, A.W.; Stone, J.R.; Guichon, P.A.M. Parameter optimization for the latest quark-meson coupling energy-density functional. *Phys. Rev. C* **2019**, *100*, 024333. [CrossRef]
132. Martinez, K.L.; Thomas, A.W.; Guichon, P.A.M.; Stone, J.R. Tensor and pairing interactions within the quark-meson coupling energy-density functional. *Phys. Rev. C* **2020**, *102*, 034304. [CrossRef]
133. Adam, C.; Martín-Caro, A.G.; Huidobro, M.; Vázquez, R.; Wereszczynski, A. Quantum skyrmion crystals and the symmetry energy of dense matter. *Phys. Rev. D* **2022**, *106*, 114031. [CrossRef]
134. Skyrme, T. A unified field theory of mesons and baryons. *Nucl. Phys.* **1962**, *31*, 556–569. [CrossRef]